JATIS Journal of Astronomical Telescopes, Instruments, and Systems

RESEARCH PAPER

Model predictive star tracking control for ground-based telescopes: the Telescopio Nazionale Galileo case

Giacomo Basile,[a,b,*] Manuel Gonzalez,[c] Alberto Petrillo,[b] Stefania Santini,[b] Salvatore Savarese,[a] and Pietro Schipani[a]

[a]INAF – Osservatorio Astronomico di Capodimonte, Naples, Italy
[b]DIETI – University of Naples Federico II, Naples, Italy
[c]INAF – FGG, TNG, Breña Baja, Spain

ABSTRACT. With the aim of improving the star tracking performance of ground-based telescopes, we deal with the design of model predictive control architecture so as to properly lead their axes while mitigating possible external disturbances affecting the control task. The proposed architecture is composed of two layers, namely, (i) a trajectory generator that determines, based on the astronomic computation, the telescope position and speed references to be tracked while ensuring that all the telescope physical constraints, in terms of speed and acceleration, are never violated; (ii) an model predictive control (MPC) controller that guarantees the optimal tracking of the desired reference behavior by providing the torque inputs for telescope axes for the achievement of star observation task. The control architecture is tailored for the tracking control problem of Telescopio Nazionale Galileo (TNG), located at La Palma (Spain). To this end, by leveraging real data measurements in specific operative scenarios, a 12-order linear system describing the TNG dynamics is identified, via the non-iterative subspace method, for the design of the second layer. Validation results confirm the goodness of the dynamical model in predicting the TNG behavior within the operative range of (80 and 90 deg) altitude position. The effectiveness of the proposed MPC-based control architecture is proven via an ad-hoc virtual testing simulation platform implemented in MATLAB and Simulink and tailored for the identified TNG model. Virtual testing results, involving the real scientific target TYC 1731-916-1, confirm the capability of the proposed solution in ensuring optimal star tracking while mitigating the wind external disturbances forces. Finally, a comparison analysis w.r.t. the state-of-the-art control approaches, i.e., Linear-Quadratic-Gaussian and Proportional-Integrator-Derivative controller, and a robustness analysis w.r.t. the model mismatch between the MPC prediction model and the simulated TNG dynamics are provided to disclose the improved tracking performance achievable via the proposed MPC-based control architecture.

 [DOI: 10.1117/1.JATIS.10.4.044011]

Keywords: ground-based telescope; telescope tracking control; axes control; model-predictive control; Telescopio Nazionale Galileo

Paper 24046G received Apr. 20, 2024; revised Oct. 8, 2024; accepted Nov. 27, 2024; published Dec. 17, 2024.

1 Introduction

Over the last few years, the increasing demand for high-performance telescopes in the study of the universe has led to the investigation of improved control architectures for advanced telescope

*Address all correspondence to Giacomo Basile, giacomo.basile@inaf.it/@unina.it

axis control.[1] Among the several control tasks, which the architectures aim at tackling, the tracking control of the telescope, i.e., the axes control problem, is one of the most critical.[2] Indeed, the problem has been deeply investigated and implemented with different hardware in previous telescopes and antenna projects.[3] The control problem aims to stabilize the position of the telescope on the scientific target to guarantee high precision and tracking performance.

More specifically, for the class of ground-based telescopes, the problem of axes control can be divided into several tasks, which include the pointing system control (i.e., the core of the tracking controller), the servo drive, and the guidance system. When designing tracking control for radio and optical ground-based telescopes, it is necessary to handle the presence of unavoidable external disturbances and noise measurements, which have to be attenuated and reduced, respectively, as well as to compensate for the gravity effects.[4] First attempts in this direction are reported in Ref. 5, where the authors designed a state-feedback control plus a feed-forward disturbance compensation gain action for solving the axes control problem of the 8.2-m very large telescope (VLT) while facing the presence of torque wind disturbance. By considering again the VLT, with the aim of improving the tracking performance, Ref. 6 proposed the same control strategy for a novel servo system. Regarding the 10-m Gran Telescopio Canarias (GTC), Ref. 7 suggested an output integral feedback position controller for solely driving motor dynamics. Conversely, for the specific case of the 3.5-m Telescopio Nazionale Galileo (TNG), Refs. 8 and 9 proposed a double-layer control system, which consists of a speed filter control loop and a proportional-integral (PI)-based position control loop, both tuned to mitigate the external wind disturbance. Another exemplary tracking controller was designed in Ref. 10 for the 17-m major atmospheric gamma-ray imaging Cherenkov telescopes, where the controller, inspired by Ref. 8, embeds a trajectory generator to deal with the physical limitation of the telescope. For the specific case of the 34-m and 70-m antennas of the NASA Deep Space Network (DSN), a double control loop, combining a Linear-Quadratic-Gaussian (LQG) regulator for the position control and a Proportional-Integral-Derivative (PID) controller for the speed dynamics, was designed in Ref. 11. However, the design does not consider the presence of external disturbance, which is an unrealistic operating condition.

Furthermore, with respect to the novel Extremely Large Telescope (ELT) projects, that is, the 30-m Thirty Meter Telescope and the 40-m European Extremely Large Telescope, Refs. 12 and 13 suggested a tracking controller, where a double PI-based control loop, combined with a low-pass filter, deals with the noise measurements, high-frequency input disturbance, and anti-gravity compensation. More recently, the tracking control problem for the green bank radio telescope has been addressed and solved in Ref. 14 via a control strategy, which exploits the pointing model parametric function approach. Finally, without considering a real-world telescope application, Ref. 15 investigated the benefits of the back-stepping adaptive control strategy in coping with the uncertainties of the model parameters dynamics and the external wind disturbance.

Based on the aforementioned state-of-the-art tracking control for ground-based telescopes, it is possible to note that most of the works mainly focused on the development of the control system rather than exploring novel control architecture solutions. Indeed, even though some works, such as Ref. 11, are based on optimal control strategies, these latter are only exploited for controlling one of the telescope dynamics, i.e., the position ones. However, the design of a novel control architecture, which also includes optimal control for the telescope speed, can further improve the tracking performance.

By leveraging the advantages of the model predictive control (MPC) approach in guaranteeing an optimal and robust tracking performance, while simultaneously dealing with multiple inputs/outputs, nonlinearities, and also satisfying the plant admissible physical constraints,[16] this work presents an MPC-based architecture for the solution of the star-tracking control problem for optical ground-based telescopes. Specifically, different from the telescope tracking state-of-the-art, which leverages two control loops for controlling the telescope position and speed, the proposed novel control solution aims at controlling both telescope axes in terms of position and speed trajectories in a unified framework while ensuring optimal performance criteria. Note that, owing to the tailored dynamical prediction model, which also includes the wind turbulence von Kármán power spectrum density (PSD) forecast, the proposed architecture is robust in the sense of performance as it is able to ensure good tracking despite the presence of measurement noise while counteracting the wind disturbance.

To this aim, the architecture consists of (i) the trapezoidal speed profile trajectory generator, which, based on the astronomical computation, determines the position and speed reference to be tracked while ensuring that all the telescope physical constraints are always not violated; (ii) an MPC strategy, which, based on the pre-processed trajectories and the estimation of the telescope dynamics, provided by an infinite horizon Kalman filter, computes the optimal telescope torque profiles for driving its axes toward the scientific target; this is done despite the presence of input external disturbance such as the wind force. Note that the Kalman filter, designed based on the effective telescope position and speed, properly mitigates the measurement noise.

Most notably, the proposed solution is tailored for the specific case of study of TNG. To this end, by leveraging real data measurements in the operative scenarios (80 and 90 deg), a 12-order linear system is identified via the non-iterative subspace method and validation results confirm the goodness of the resulting dynamical model in predicting the TNG behavior in the appraised functioning conditions. The resulting TNG dynamics represent the basis of the control architecture design, whose effectiveness is evaluated via virtual testing simulations for different scientific targets, including the TYC 1731-916-1 real star. The results obtained through an own-made advanced simulation platform (realized in MATLAB and Simulink) confirm the capability of the proposed solution in ensuring optimal star tracking while mitigating the wind external disturbance forces. Moreover, to better highlight the advantages of the proposed MPC-based control solution, a comparison analysis with respect to state-of-the-art control approaches, that is, LQG[17] and PID controller,[12] discloses the improved achievable tracking performance, whereas a robustness analysis w.r.t. the model mismatch between the identified TNG model exploited as MPC-based predictor and plant is reported to show the limits of the proposed control architecture.

Finally, the paper is organized as follows. Section 2 presents the problem statement, whereas the proposed MPC-based tracking control architecture is designed in Sec. 3. Virtual testing, tailored for TNG (hence including its identification and validation procedure) in Sec. 4, discloses the goodness of tracking performance, and comparison results also highlight its advantages. Conclusions are drawn in Sec. 5.

1.1 Nomenclature and Notations

Throughout this paper, $\mathbb{R}$ and $\mathbb{N}$ stand for the set of real and natural numbers, respectively. We use $\mathbb{R}^{m\times n}$ to denote the set of $m \times n$ real matrices, whereas $\mathbb{S}^n$ is the set of symmetric matrices of order n. Given a symmetric matrix $M \in \mathbb{S}^n$, $M \geq 0$ ($M > 0$) means that the matrix is positive semidefinite (positive definite). The transpose operation of a generic matrix $A \in \mathbb{R}^{n\times n}$ is indicated via $A^\intercal$. I_n and $0_{n\times m}$ are the identity matrix of order n and the null matrix of dimensions $n \times m$, respectively.

Given a vector $x \in \mathbb{R}^n$, $\|x\|_2 = (x^\intercal x)^{1/2}$ defines the Euclidean norm of the vector x, whereas $\|x\|_Q = (x^\intercal Q x)^{1/2}$ denotes the Euclidean norm of the vector x weighted by the matrix $Q \in \mathbb{R}^{n\times n}$.

Furthermore, given a bounded trajectory $x(t) \in \mathbb{R}$, $x_{\min}$ and $x_{\max}$ define its minimum and maximum values, respectively.

Finally, saturation $(x_{\min}, x_{\max})$ refers to the following equation:

$$x(t) = \text{saturation}(x_{\min}, x_{\max}) = \begin{cases} x_{\max} \Leftrightarrow x(t) \geq x_{\max} \\ x(t) \Leftrightarrow x_{\min} \leq x(t) \leq x_{\max} \\ x_{\min} \Leftrightarrow x(t) \leq x_{\min} \end{cases}. \tag{1}$$

2 Tracking Control for Ground-Based Telescope: Problem Statement

Consider a ground-based telescope equipped with on-board sensors, such as the tachometers and encoders for the measurement of its altitude and azimuth velocities and positions, and a scientific target star to be tracked, with features that are expressed, via the astronomical computation, with respect to the azimuth coordination system, that is, the altitude angle $\vartheta^\star(t)$[deg] and the azimuth angle $\varphi^\star(t)$[deg].

The aim of this work is to design a novel MPC-based control architecture that is able to drive the telescope axes for the optimal achievement of star tracking. The control architecture is

designed to fulfill the following requirements: (i) computation of the appropriate telescope axes position and speed trajectories such that all the telescope physical constraints, in terms of speed and acceleration, are always not violated; (ii) computation of the optimal telescope control torque, which ensures the high tracking performance for both the altitude and azimuth axes, while guaranteeing robust performance despite the presence of measurement noise and external disturbance affecting the telescope dynamics.

2.1 Ground-Based Telescope Dynamics

The behavior of a ground-based telescope is mainly described by its measurable velocities $y(t) = [\dot{\vartheta}(t), \dot{\varphi}(t)]^\intercal \in \mathbb{R}^2$ in the azimuth coordination system, being $\dot{\vartheta}(t)[\text{deg}/\text{s}]$ the altitude angular speed and $\dot{\varphi}(t)[\text{deg}/\text{s}]$ the azimuth angular speed. Within this framework, according to Ref. 18, the ground-telescope dynamical behavior can be described by the following linear model:

$$\dot{x}(t) = Ax(t) + B(u(t) - \delta(t))$$
$$y(t) = Cx(t) + \omega$$

with

$$A = \begin{bmatrix} A_e & 0_{6\times6} \\ 0_{6\times6} & A_a \end{bmatrix} \quad B = \begin{bmatrix} B_e & 0_{6\times1} \\ 0_{6\times1} & B_a \end{bmatrix} \quad C = \begin{bmatrix} C_e & 0_{1\times6} \\ 0_{1\times6} & C_a \end{bmatrix}, \tag{2}$$

where $x(t) = [x_e(t)x_a(t)]^\intercal \in \mathbb{R}^{12}$ is the flexible dynamics of the telescope, being $x_e(t)$ the state vector related to altitude dynamics, whereas $x_a(t)$ is the one related to azimuth dynamics; $u(t) = [\tau_e(t), \tau_a(t)]^\intercal [Nm] \in \mathbb{R}^2$ is the control input vector representing the torque commands along the altitude axis, i.e., $\tau_e[\text{Nm}]$, and the azimuth axis, i.e., $\tau_a[\text{Nm}]$; $\delta(t)[\text{Nm}] \in \mathbb{R}^2$ is the input wind external disturbance; $\omega \in \mathbb{R}^{2\times1}$ is the measurements of white noise affecting the output vector; $A \in \mathbb{R}^{12\times12}$ is the overall dynamical matrix of the telescope being $A_e \in \mathbb{R}^{6\times6}$ and $A_a \in \mathbb{R}^{6\times6}$ the dynamical matrices related to altitude and azimuth axes dynamics, respectively; $B \in \mathbb{R}^{12\times2}$ is the input telescope matrix where $B_e \in \mathbb{R}^{6\times1}$ and $B_a \in \mathbb{R}^{6\times1}$ map the relation between the torque commands along the altitude and azimuth axes with the related states $x(t)$, respectively; $C \in \mathbb{R}^{2\times12}$ is the output telescope matrix with blocks $C_e \in \mathbb{R}^{1\times6}$ and $C_a \in \mathbb{R}^{1\times6}$ that represent the altitude and the azimuth outputs matrices, respectively.

Remark 1: *The value of the matrices A, B, and C strongly depends on the specific appraised telescope, and they can be tailored by exploiting the identification procedure suggested in Ref. 18. The specific value for the TNG case of the study can be found in* Sec. 4.1.

The matrices describing the telescope dynamics are such that the following assumptions hold.

Assumption 1: The pair (A, B) is stabilizable.

Assumption 2: The pair (A, C) is observable.

Assumption 3: C is a full-row rank matrix.

According to Ref. 19, the wind external disturbance $\delta(t)$ is modeled via the von Kármán wind PSD as

$$\delta(t) = \sum_{j=1}^{D} \sqrt{2\alpha S_\tau(f_j)\Delta f}\ \cos(2\pi f_j t + \phi_j), \tag{3}$$

with $D \in \mathbb{N}$ the number of the contributed frequency samples; α is a scale intensity factor; $\Delta f[1/\text{s}]$ is the frequency resolution; f_j is the j'th element of the numerical sequences $f(j) = \{j\Delta f\}$ being $j \in (1, D)$; $\phi_j = \mathcal{N}(\mu, \sigma)[\text{deg}]$ $(\forall\ j = 1, \cdots, D)$ is the initial phase computed through a random uniform distribution with mean μ and standard deviation σ. The torque von Kármán PSD $S_\tau(f_j)$ is described by

$$S_\tau(f_j) = 4\left(\frac{\overline{\tau}}{\overline{v}}\right)^2 S_v(f_j)\chi(f_j)^2, \tag{4}$$

where $\overline{\tau}$[Nm] is the wind mean torque disturbance, $\overline{v}$[m/s^2] is the mean wind speed, $S_v(f_j)$ is the von Kármán speed wind PSD, and $\chi(f_j)$ is the aerodynamic correction factor.

In detail, $S_v(f_j)$ is computed as

$$S_v(f_j) = 4(\mathcal{I}\overline{v})^2 \frac{\Gamma}{\overline{v}} \frac{1}{\left(1+70.78\left(f_j \frac{\Gamma}{\overline{v}}\right)^2\right)^{5/6}}, \tag{5}$$

where $\mathcal{I}$ is the wind disturbance intensity and Γ is the outer scale of the wind disturbance.

Besides, $\chi(f_j)$ can be derived as

$$\chi(f_j) = \frac{1}{1+\left(2f_j \frac{\sqrt{\Lambda}}{\overline{v}}\right)^{4/3}}, \tag{6}$$

where Λ[m^2] is the telescope area exposed to the wind disturbance.

2.2 Problem Statement

Now, it is possible to formulate the tracking control problem as follows:

Problem: $\mathcal{C}$ Consider the ground-based telescope dynamics as in Eq. (2). Let the scientific target star be expressed, within the azimuth coordination system, in terms of the vector $y^\star(t) = [\vartheta^\star(t), \varphi^\star(t)]^\intercal$. Design an MPC-based tracking control architecture such that the telescope torques $u(t) = [\tau_e, \tau_a]^\intercal$ can properly drive the altitude and azimuth axes toward the star scientific target by avoiding violating the admissible physical constraints and fulfilling the following control objective:

$$\lim_{t\to\infty} \left\| y^\star(t) - \int_0^t y(\rho)\mathrm{d}\rho \right\|_2 = 0, \tag{7a}$$

$$\lim_{t\to\infty} \left\| \dot{y}^\star(t) - y(t) \right\|_2 = 0, \tag{7b}$$

despite the presence of the input wind disturbance $\delta(t)$ and noise measurements ω.

3 MPC-Based Tracking Control Architecture Design

To solve problem $\mathcal{C}$, we design the double-layer control architecture in Fig. 1. The proposed solution consists of

- The trajectory generator, which, given the scientific star target to be tracked, i.e., $y^\star(t) = [\vartheta^\star(t), \varphi^\star(t)]^\intercal$, computes the safe and physical admissible reference position and velocity trajectories for telescope altitude and azimuth axes, i.e., $\overline{y}_p(t) = [\overline{\vartheta}(t), \overline{\varphi}(t)]^\intercal$ and $\overline{y}_s(t) = [\dot{\overline{\vartheta}}(t), \dot{\overline{\varphi}}(t)]^\intercal$, respectively.

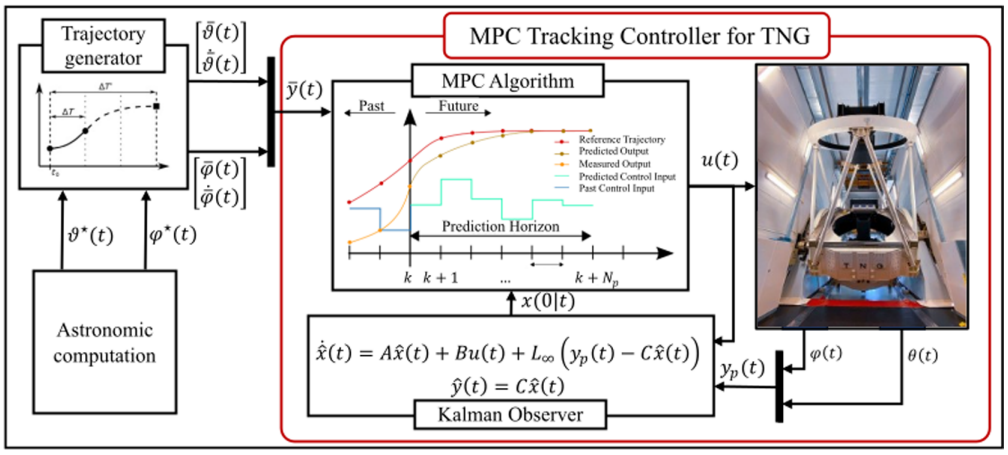

Fig. 1 Overview of the MPC-based tracking architecture.

- The *MPC*-based tracking controller, which, combining an infinite horizon Kalman observer and the model predictive control algorithm, ensures the computation of the optimal torque profile $u(t)$ that guarantees the optimal and robust tracking of the $\overline{y}_p(t)$ and $\overline{y}_s(t)$, despite the presence of input external disturbance $\delta(t)$ and output measurement noise ω

In doing so, the control objectives in Eqs. (7a) and (7b) are achieved. In Sec. 3.1, we detail the design of the two layers composing the optimal tracking control architecture in Fig. 1.

3.1 Trajectory-Generator

According to Refs. 20–22, the trajectory generator is designed by leveraging the trapezoidal speed profile approach. Specifically, given the star position $y^\star(t)$, it generates: (i) the telescope trapezoidal speed profile $\overline{y}_s(t) = [\dot{\overline{\vartheta}}(t), \dot{\overline{\varphi}}(t)]^\intercal$ and (ii) the physical admissible position trajectories $\overline{y}_p(t) = [\overline{\vartheta}(t), \overline{\varphi}(t)]^\intercal$.

Accordingly, telescope velocities keep a constant maximum value $v_{\max}$ or increase and decrease at the fixed maximum allowable acceleration $\pm a_{\max}$. Thus, according to Ref. 22, the desired trajectories $\overline{y}_p(t)$ and $\overline{y}_s(t)$ are computed as

$$\dot{\overline{y}}_p(t) = \overline{y}_s(t) \quad \overline{y}_s(t) = \text{saturation}(v_a(t), \min(v_d(t), v_{\max})), \tag{8}$$

where $v_a(t)$ is the speed during the acceleration phase, whereas $v_d(t)$ is the one during the deceleration phase. The acceleration ramp can be expressed as

$$v_a(t) = v(t - \Delta t) + a_{\max}\Delta t, \tag{9}$$

where Δt is the sampling time, whereas $v(t - \Delta t)$ is the measured telescope speed at time instant $t - \Delta t$. The deceleration ramp can be computed as[20]

$$v_d(t) = \dot{y}^\star(t) + \text{sign}(\varepsilon(t))\sqrt{2a_{\max}|\varepsilon(t)|}, \tag{10}$$

where $\dot{y}^\star(t)$ is the reference velocity of the target star, computed via the astronomical computation; $\varepsilon(t) = y^\star(t) - \bar{y}(t)$ represents the error between the planned trajectories and the star positions. Note that Eq. (10) is valid for an arbitrary instant and represents the initial velocity of an ideal decelerating motion, which would drive ε to 0 with a final velocity equal to $v^\star(t)$. Therefore, $v_d(t)$ is the velocity limit, which determines the moment for the starting of the deceleration phase.

In doing so, the velocity trajectories can initially increase at the fixed maximum acceleration value $a_{\max}$ until reaching, or the maximum admissible speed $v_{\max}$—if this latter is still less than $v_d(t)$—or start decelerating according to Eq. (10).

The outputs $\overline{y}_p(t) = [\overline{\vartheta}(t), \overline{\varphi}(t)]^\intercal$ and $\overline{y}_s(t) = [\dot{\overline{\vartheta}}(t), \dot{\overline{\varphi}}(t)]^\intercal$ of the trajectory generator, i.e., the planned altitude $\overline{\vartheta}(t)$, azimuth $\overline{\varphi}(t)$ positions, and its computed trapezoidal speed profiles, i.e., $\dot{\overline{\vartheta}}(t)$ and $\dot{\overline{\varphi}}(t)$, represent the desired behavior to be tracked by the MPC-based tracking controller.

3.2 MPC-Based Tracking Controller

Given the reference behavior to be tracked, the tracking controller layer (see the red box in Fig. 1) aims at ensuring an optimal, robust, and high-performance tracking of $\overline{y}_p(t)$ and $\overline{y}_s(t)$ by computing the telescope control $u(t)$ according to the MPC method, hence achieving the control goals in Eqs. (7a) and (7b).

To this end, an infinite horizon Kalman filter observer is also exploited for the estimation of the whole telescope dynamics $\hat{x}(t)$ to let the MPC algorithm properly compute the optimal torque action $u(t)$ in Eq. (2) to be imposed on the ground-based telescope.

3.2.1 *Infinite horizon Kalman filter*

As the ground-based telescope model in Eq. (2) is not affected by any process noise, and hence, its dynamics are such that the measurement noise is uncorrelated to process one, an infinite horizon Kalman state observer is designed to provide the estimation of the telescope state variables, i.e., $\hat{x}(t) \in \mathbb{R}^{12}$.

Specifically, the Kalman filter is described by the following dynamical system:

$$\begin{aligned}\dot{\hat{x}}(t) &= A\hat{x}(t) + Bu(t) + L_\infty(y(t) - \hat{y}(t))\\ \hat{y}(t) &= C\hat{x}(t),\end{aligned} \tag{11}$$

where $L_\infty \in \mathbb{R}^{12\times 2}$ is the gain observer matrix to be computed according to the optimality criteria for the expected value of the estimation error.[23]

In doing so, consider the estimation error $\hat{e}(t) = x(t) - \hat{x}(t) \in \mathbb{R}^{12}$, its expected covariance matrix $\tilde{P}(t) = \mathbb{E}[\hat{e}(t)\hat{e}(t)^\intercal] \in \mathbb{R}^{12\times 12}$, and the covariance matrix V as

$$V = \begin{bmatrix} \tilde{Q} & 0_{14\times 2} \\ 0_{2\times 14} & \tilde{R} \end{bmatrix},$$

where $\tilde{Q} \geq 0 \in \mathbb{S}^{12}$ is the diagonal matrices weighting the estimation error states and $\tilde{R} > 0 \in \mathbb{S}^2$ the one weighting the output measurements.

Under Assumptions 2–3, according to the well-known procedure,[23] the matrix gains observer L_∞ is computed as follows:

$$L_\infty = \tilde{P}_\infty C^\intercal R^{-1}, \tag{12}$$

where $\tilde{P}_\infty$ is the unique solution of the stationary Riccati equation:

$$0 = A\tilde{P}_\infty + \tilde{P}_\infty A^\intercal + \tilde{Q} - \tilde{P}_\infty C^\intercal \tilde{R} C \tilde{P}_\infty. \tag{13}$$

Note that, as the altitude and azimuth dynamics are decoupled, the Kalman optimal gain is decomposed as

$$L_\infty = \begin{bmatrix} L_e & 0 \\ 0 & L_a \end{bmatrix},$$

where the matrices L_e and L_a are related to the altitude and azimuth dynamics, respectively.

3.2.2 *MPC control design*

Considering the desired set point $\overline{y}(t) = [\overline{\vartheta}(t), \overline{\varphi}(t), \dot{\overline{\vartheta}}(t), \dot{\overline{\varphi}}(t)]^\intercal$ as imposed by the trajectory generator and the telescope state estimation $\hat{x}(t)$, the MPC iteratively computes, over a time horizon $(t, t + T_p]$ (where T_p is the prediction horizon), the optimal input torque $u(t)$ driving the telescope axes at time t. More specifically, to track the reference set-point $\overline{y}(t)$, the torque input is computed based on optimality criteria (e.g., a quadratic cost function) and by leveraging the prediction model in Eq. (2) over $(t, t + T_p]$. In doing so, the optimal MPC control problem is first formulated and solved over the time horizon $(t, t + T_p]$, namely, the so-called MPC open control loop. Then, we present the iterative mechanism, which enables the control input to adapt to the actual prediction, that is, the MPC closed loop.[24]

MPC open control loop design. With the aim of predicting the position and velocity dynamics of the telescope, we consider the following dynamical system:

$$\begin{aligned}\dot{x}_m(t) &= A_m x_m(t) + B_m(u(t) - \delta(t))\\ y_m(t) &= C_m x_m(t),\end{aligned} \tag{14}$$

where $x_m(t) = [y(t), x(t)]^\intercal \in \mathbb{R}^{14}$ and

$$A_m = \begin{bmatrix} 0_{14\times 2} & C \\ & A \end{bmatrix} \quad B_m = \begin{bmatrix} 0_{2\times 2} \\ B \end{bmatrix} \quad C_m = \begin{bmatrix} I_2 & 0_{2\times 12} \\ 0_{2\times 2} & C \end{bmatrix}. \tag{15}$$

Denote with $T_p \in \mathbb{R}$ the prediction horizon used for solving the optimal local control problem in the time interval $(t, t + T_p]$. Instead, the control horizon $T_c \in \mathbb{R}$ (being $T_c \leq T_p$) determines the computed control command to be imposed on the telescope axes over the time interval $(t, t + T_c]$. The notation $x_m(\cdot\,|t)$ stands for the trajectory of x_m over the prediction horizon $(t, t + T_p]$ at the time instant t, whereas $x_m(\rho|t)$ with $\rho \in (0, T_p]$ indicates the computed value of x_m at time $t + \rho$. Moreover, we define three different telescope trajectories, namely,

$(\cdot)^p$ for the one predicted via Eq. (14), $(\cdot)^\heartsuit$ for the optimal desired trajectory, and $(\cdot)^a$ for the assumed trajectory. More specifically, as the desired trajectory is known over the prediction horizon $(t, t+T_p]$, we assume this latter to be computed via the trajectory generator as in Eq. (8), that is, $y^\heartsuit(\cdot\,|t) = \overline{y}(\cdot\,|t)$.

Hence, the local open-loop optimal control problem for the ground-based telescope can be formalized as follows:

Problem: $\mathcal{F}$ At time t, find

$$\min_{u^p(\cdot|t)} \int_t^{t+T_p} l(y_m^p(\rho|t), u^p(\rho|t), y_m^a(\rho|t), \overline{y}^a(\rho|t))\mathrm{d}\rho, \tag{16a}$$

s.t.,

$$x_m^p(\rho|t) = A_m x_m^p(\rho|t) + B_m(u^p(\rho|t) - \delta^p(\rho)), \tag{16b}$$

$$y_m^p(\rho|t) = C_m x_m^p(\rho|t), \tag{16c}$$

$$\delta^p(\rho) = \sum_{j=1}^{D} \sqrt{2\alpha S_\tau(f_j)\Delta f}\ \cos(2\pi f_j \rho + \phi_j), \tag{16d}$$

$$x_m^p(0|t) = \hat{x}_m(t), \tag{16e}$$

$$u^p(\rho|t) \in [\, u_{\min} \quad u_{\max}\,], \tag{16f}$$

$$y_m^p(T_p|t) = \overline{y}^a(T_p|t) - y^a(T_p|t), \tag{16g}$$

$$u(T_p|t) = \tilde{h}(T_p|t), \tag{16h}$$

where $u^p(\cdot\,|t)$ denotes the unknown control trajectory to be optimized; $u_{\min}$ and $u_{\max}$ represent the maximum admissible values for the control input, respectively. Note that additional constraints related to the azimuth and altitude position and speed are not considered in the MPC formulation because the designed trajectory generator always computes admissible reference trajectories for the telescope dynamics. $\tilde{h}(\cdot)$ is the desired final value for the control input for the counteraction of the resistance forces, that is, the wind disturbance, at time instant T_p. Note that, it is computed from the prediction model Eq. (2) by imposing the tracking equilibrium condition, i.e., $\tilde{h}(T_p|t) = K_r \bar{y}^a(T_p|t) + K_f y_m^a(T_p|t) + \delta(T_p)$ being $K_r \in \mathbb{R}^4$ and $K_f \in \mathbb{R}^4$ the feed-forward and the feedback gains, respectively, which should be properly selected.

The cost function $l(\cdot)$ in Eq. (16a) at time instant ρ and evaluated from the instant t is defined as

$$l(\cdot) = \|y_m^p(\rho|t) - \overline{y}(\rho|t)\|_Q + \|u^p - \tilde{h}(x_m^p(T_p|t))\|_R + \|y_m^p(T_p|t) - \overline{y}^a(T_p|t)\|_F, \tag{17}$$

where $Q \geq 0 \in \mathbb{S}^4$ penalizes the output error from the desired equilibrium, $R > 0 \in \mathbb{S}^2$ penalizes the input error, and $F \geq 0 \in \mathbb{S}^2$ represents the strength at the instant T_p to maintain the telescope output as close as possible to the assumed desired trajectories.

Tracking model predictive control closed-loop algorithm. The tracking MPC algorithm, allowing the derivation of the optimal torque trajectory $u(\cdot\,|t)$ over the control horizon $(t, t+T_c]$, for the ground-based optical telescope is developed according to the following iterative procedure:

1. Initialization: At $t = 0$, based on the target star trajectory $y^\star(\cdot\,|t)$, and the pre-processed trajectories $\overline{y}(\cdot\,|t)$, we initialize the assumed variables as

$$\begin{cases} u^a(\cdot\,|t) = \tilde{h}(0|t) \\ y^a(\cdot\,|t) = C_m x_m^p(0|t), \end{cases} \tag{18}$$

   where x_m^p is the trajectory predicted via Eq. (14).
2. First step: At any $t > 0$, based on the estimated current Kalman filter state $\hat{x}(t)$, the assumed state $x_m^a(\rho|t)$ and the assumed star trajectory $\bar{y}^a(\rho|t)$ solve the optimal control problem $\mathcal{F}$, hence obtaining the optimal control effort $u^\heartsuit(\cdot\,|t)$. Based on this latter, the optimal state trajectory $x_m^\heartsuit(\cdot\,|t)$ is computed via the telescope model in Eq. (14).

3. Second step: Compute the assumed control input for the next open loop control problem, namely, the ones over the horizon $[t+\Delta t, t+\Delta t+T_p]$, being $\Delta t \in \mathbb{R}$ an arbitrary sample time, by disposing the optimal terms within $T_p - \Delta t$ and adding an additional one for the instant T_p, that is, ****

$$u^a(\rho|t+\Delta t) = \begin{cases} u^{\heartsuit}(\rho|t) & \rho \in (0, T_p - \Delta t] \\ \tilde{h}(T_p|t) \end{cases}. \tag{19}$$

Then, we compute the corresponding assumed state and output for $\rho \in (0, T_p - \Delta t]$, as

$$\begin{aligned} \dot{x}_m^a(\rho|t+\Delta t) &= A_m x_m^a(\rho|t+\Delta t) + B_m(u^a(\rho|t+\Delta t) - \delta^a(k)), \\ y_m^a(\rho|t+\Delta t) &= C_m x_m^a(\rho|t+\Delta t), \\ x_m^a(0|t+\Delta t) &= x_m^{\heartsuit}(1|t). \end{aligned} \tag{20}$$

4. Third step: receive $\overline{y}^a(\rho|t+\Delta t)$ from the trajectory generator.
5. Fourth step: impose the optimal control input within the time interval $(t, t+T_c]$, i.e., $(((u(t) = u^{\heartsuit}(\rho|t)$ with $\rho \in (0, T_c]$.
6. Fifth step: increment t until $t+T_c$ and go to step 1.

Remark 2: *[MPC Closed-loop Stability] The stability of the telescope closed-loop system under the action of the MPC control in* Eq. (16a) *can be derived by following well-known results in the control theory literature (e.g., see Refs.* 16 *and* 24–26*). Namely, the MPC stability is mathematically ensured if the plant satisfies the following assumptions: (A1) the nonlinear vector field in the plant model is twice continuously differentiable; (A2) the control input region is compact and convex and contains the origin; (A3) the Jacobian linearization of the nonlinear system is stabilizable; (A4) the optimal control problem is feasible at time* $t = 0$*. Note that, as the telescope dynamical model* Eq. (2) *is linear and satisfies Assumptions 1, A1 and A3 surely hold. Moreover, the assumed control input in* Eq. (19)*, thanks to the terminal input constraint* Eq. (16h)*, which compensates for the wind turbulence effect* $\delta(t)$*, satisfies A2 by construction because its admissible region is defined as* $\mathcal{U}: \{u(\cdot\,|t) \in \mathbb{R}: u_{\min} \leq u(\cdot\,|t) \leq u_{\max}\}$*. Finally, A4 holds for the selection of the telescope's initial value for the torque within the telescope's physical limits.*

Remark 3: *As the proposed MPC approach belongs to the class of terminal constraint MPC,*[24] *constraint* Eq. (16h) *plays a crucial role in the stability of the MPC control algorithm in a twofold way*[16,24]*: (i) it aims at compensating the wind disturbance* $\delta(t)$ *under the assumption that the von Kármán PSD model fits the real wind data, hence ensuring the robustness of telescope w.r.t. the wind disturbance; (ii) the proper choice of* K_r *and* K_f *(tuned for instance via pole-placement and LQR techniques*[17,27]*) guarantees the telescope tracking error* $e(t) = \overline{y}(t) - y_m(t)$ *goes toward zero as* $t \to \infty$ *as also explicitly imposed by the constraint* Eq. (16g)*. Finally, note that this latter is also necessary to formally guarantee that the functional cost is convex and optimizable at each iteration step.*[16]

4 Case of Telescopio Nazionale Galileo

In this section, we tailor the design of the proposed control architecture in Sec. 3 to the Telescopio Nazionale Galileo, located at "Roque de los Muchacho," La Palma (Spain). To this aim, an identification procedure is first carried out to obtain the TNG dynamics as in Eq. (2), which are exploited for simulation purposes in the MATLAB platform. This latter is used for the validation of the proposed control architecture, and the implementation details of the MPC-based control architecture are also provided.

Finally, an extensive simulation analysis, involving the real scientific target TYC 1731-916-1 and including a comparison w.r.t. other state-of-the-art control architectures plus a robustness analysis w.r.t. model mismatch, discloses the benefits and the advantages of the proposed solution.

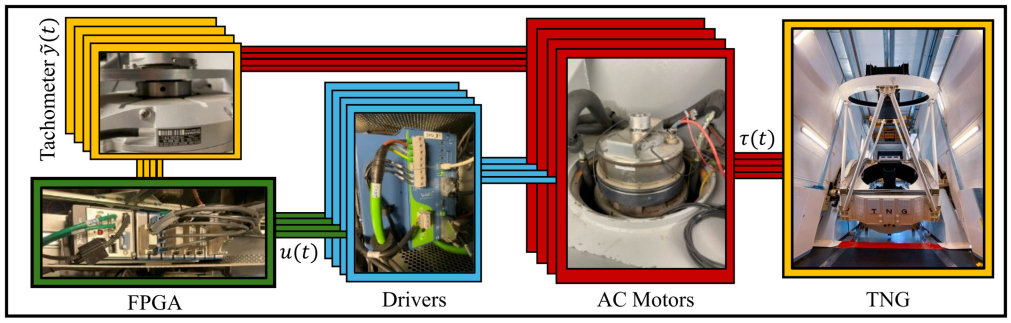

Fig. 2 Schematic overview for data acquisition experimental set-up for altitude and azimuth axes.

4.1 TNG Dynamics Identification

By levering the real data in Ref. 28, we derive the control-oriented model for TNG able to reproduce its input/output (I/O) behavior as in Eq. (2) such that it can be exploited for the designing of the proposed MPC-based tracking control solution.

It is worth noting that, due to the morphology of the area of "Roque de lo Muchachos" and the TNG observatory structure, the PSD von Kármán model can represent the wind disturbance.[29] For this purpose, data are recorded via the experimental set-up depicted in Fig. 2. It consists of (i) four Heidenhain RPN 886 tachometers (yellow squares) for the measurement of TNG velocity and position trajectories; (ii) four DC brush-less permanent magnets electric motors with 32 pole pair stator, three phases at $180[V]$ voltage alternative current (VAC) (red squares) for the imposition of the real torque to the TNG; (iii) four Aerotech Soloist Hpe-50 drivers (blue squares) for the providing of the suitable voltages to the actuators such that the desired torques, computed by the control unit (CU), are ensured; (iv) the field-programmable gate array (FPGA) (green square), i.e., the CU of the National Instrument compact-RIO (NI cRio) 9039 for the controlling of the TNG telescope. Note that, the presented hardware is replicated for both axes unless the FPGA aims at controlling both simultaneously.

The exploited data have been acquired by exciting the TNG real system via a mean zero white noise torque, at a sample time of 0.002 (namely, the control unit sample time) and recording the altitude and azimuth speed trends $\tilde{y}(t) = [\dot{\tilde{\vartheta}}(t), \dot{\tilde{\varphi}}(t)]$ via the on-board equipped tachometers. Note that, the ground telescope presents different operative scenarios depending on the altitude dynamics. In this work, data measurements refer to the altitude operative range of 80 and 90 deg.

The system identification problem is here formulated as an optimization task where the objective is to find the set of linear state space matrices A, B, C, and D in Eq. (2) such that the prediction error between the plant outputs, i.e., the measured data $\tilde{y}(t)$, and the model output, computed based on the known inputs, i.e., $y(t)$, is minimized. Specifically, by assuming the TNG model as a black-box system, the exploited identification procedure leverages the non-iterative subspace method to properly compute the TNG linear state space model, and the prediction error minimization approach to improve the accuracy of the identified matrices.[30]

The resulting TNG matrices are identified as in Table 1 and are such that Assumptions 1 and 2 hold, allowing the design of the proposed control approach. In doing so, being D a null matrix, the identified TNG linear model presents a root-mean-square-error (RMSE) of 6×10^{-4} deg and of 0.002 deg for the altitude and azimuth axes, respectively, hence highlighting a good prediction capability.

The good prediction capability is also confirmed by Figs. 3(c)–3(f) where the time history of the altitude prediction error $\tilde{\vartheta}(t) - \vartheta(t)$ [deg] and azimuth prediction error $\tilde{\varphi}(t) - \varphi(t)$ [deg] are reported, respectively.

The reliability of the identified model in correctly predicting the TNG behavior is also disclosed in Figs. 3(a), 3(b), 3(d), and 3(e). Specifically, the magnitude of the input–output measurements w.r.t. the magnitude of the frequency response of the identified altitude TNG dynamics is reported in Fig. 3(a), whereas their phase diagrams are reported in Fig. 3(b). The same behavior can be appreciated for the azimuth TNG dynamics in Figs. 3(d) and 3(e).

Table 1 TNG linear state space matrices.

$$A_e = \begin{bmatrix} -21.59 & 374.92 & 522.37 & 174.12 & 85.41 & -448.44 \\ -363.16 & -4.54 & -360.01 & -60.97 & 47.62 & 193.88 \\ -321.21 & 331.22 & -127.72 & -588.27 & 7.52 & 497.92 \\ -414.77 & -64.38 & 1353.24 & -519.62 & 232.46 & 1087.37 \\ -39.80 & -33.56 & -70.82 & 2.58 & -4.57 & -371.65 \\ 180.89 & -140.82 & -15.70 & -682.73 & 311.77 & 47.47 \end{bmatrix} \quad B_e = \begin{bmatrix} 0.0072 \\ -0.0048 \\ -0.0048 \\ -0.0162 \\ 0.0028 \\ -0.0131 \end{bmatrix} \quad C_e = \begin{bmatrix} 10614.83 \\ 6577.62 \\ 3222.93 \\ 334.27 \\ 846.50 \\ 292.02 \end{bmatrix}^T$$

$$A_a = \begin{bmatrix} 226.76 & 959.76 & 478.91 & 174.65 & 1114.18 & -942.69 \\ -328.81 & 328.57 & 679.15 & 130.25 & 145.20 & -132.75 \\ 537.10 & -481.54 & 114.51 & 153.75 & 470.65 & -234.11 \\ -306.69 & -133.06 & -209.26 & 61.65 & -94.12 & -14.57 \\ -595.34 & -1032.85 & -2433.71 & 183.40 & -1354.58 & 1483.91 \\ 250.63 & 321.98 & 945.13 & 4.65 & 396.46 & -458.34 \end{bmatrix} \quad B_a = \begin{bmatrix} 0.0011 \\ 0.0004 \\ -0.0006 \\ -0.0013 \\ -0.0020 \\ 0.00057 \end{bmatrix} \quad C_a = \begin{bmatrix} -17490.42 \\ -13275.20 \\ 9480.43 \\ -3518.08 \\ -1713.89 \\ 24.57 \end{bmatrix}^T$$

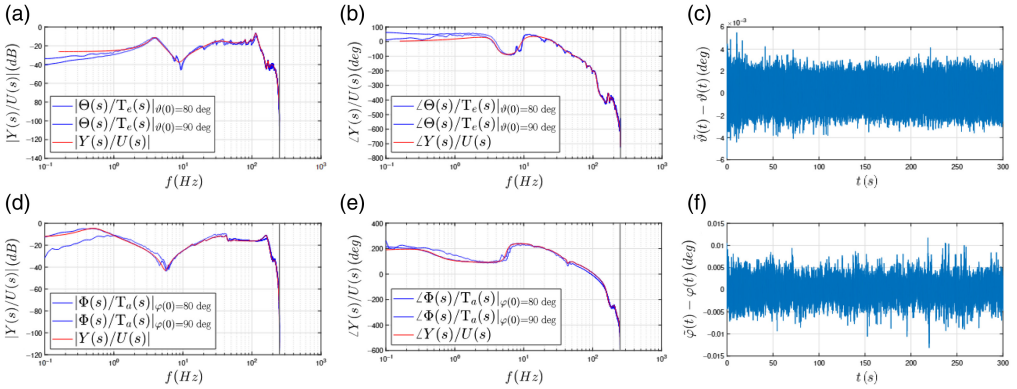

Fig. 3 Identification results within the operative range $\vartheta \in (80, 90\ \text{deg})$: (a) comparison of the magnitude measured data and the frequency response of the identified altitude axes model; (b) comparison of the phase measured data and the phase diagram of the identified altitude axes model; (c) time history of the prediction error $\tilde{\vartheta}(t) - \vartheta(t)$; (d) comparison of the magnitude measured data and the frequency response of the identified azimuth axes model; (e) comparison of the phase measured data and the phase diagram of the identified azimuth axes model; (f) time history of the prediction error $\tilde{\varphi}(t) - \varphi(t)$.

Remark 4: *From the experimental analysis of the TNG behavior, we noted, at the low-frequency range, a mismatching between the frequency responses of measurements and the identified model [see* Figs. 3(a), 3(b), 3(d), and 3(e)]. *This is because TNG dynamics are affected by nonlinearities, such as balancing issues (caused by the TNG aging) and its strong static friction when passing from a specific position to another one with non-zero speed. Moreover, the frequency mismatches are justified by the exploited identification algorithm with the aim of minimizing the prediction error trend over the time domain.*

4.2 MPC-Based Tracking Control Architecture: Implementation Details

With the aim to test and validate the proposed control algorithm, the whole architecture is implemented by considering a sample time of $\Delta t = 0.002\,[s]$, according to the already-installed TNG hardware architecture.[31]

Specifically, all the differential equations are integrated via the Runge–Kutta algorithm. In doing so, the trajectory generator and Kalman Filter observer present the same structure presented in Secs. 3.1 and 3.2.1, respectively, whereas the MPC control algorithm is discretized according to the chosen sample time.

Specifically, the prediction horizon becomes $[t, t + N_p\Delta t]$ where N_p is the number of prediction samples, i.e., $N_p = T_p/\Delta t$, whereas the control horizon becomes $[t, t + N_c\Delta t]$ where $N_c = T_c/\Delta t$ $(N_c \leq N_p)$ is the number of control samples imposed to the telescope.

Then, based on the measured/estimated value at time t, indicated with $x_m(k|t)$ $\forall\ k \in (0, \cdots, N_p - 1)$, the k'th value of x_m is over the horizon, i.e., the one computed at time instant $t + k\Delta t$, where $k = 0, \cdots, N_p - 1$ is the index of the sample within the horizon. In so doing, the local open-loop MPC control problem for ground-based telescope can be recast in the discrete implementation form as: At time t, find

$$\min_{u^p(\cdot|t)} \sum_{k=0}^{N_p-1} \|y_m^p(k|t) - \overline{y}(k|t)\|_Q + \|u^p(N_p|t) - \tilde{h}(x_m^p(N_p|t))\|_R + \|y_m^p(N_p|t) - \overline{y}_m^a(N_p|t)\|_F, \tag{21a}$$

s.t.,

$$x_m^p(k+1|t) = A_m x_m^p(k|t) + B_m(u^p(k|t) - \delta^p(k)), \tag{21b}$$

$$y_m^p(k|t) = C_m x_m^p(k|t), \tag{21c}$$

$$\delta^p(k) = \sum_{j=1}^{D} \sqrt{2\alpha S_\tau(f_j)\Delta f}\ \cos(2\pi f_j k + \phi_j), \tag{21d}$$

$$x_m^p(0|t) = \hat{x}_m(t), \tag{21e}$$

$$u^p(k|t) \in [\, u_{\min} \quad u_{\max}\,], \tag{21f}$$

$$y_m^p(N_p|t) = \overline{y}^a(N_p|t) - y^a(N_p|t), \tag{21g}$$

$$u(N_p|t) = \tilde{h}(x_m^p(N_p|t)). \tag{21h}$$

Note that Eq. (21b) is also integrated via Runge–Kutta over the prediction horizon. MPC parameters set-up is reported in Table 2, whereas the input constraints and sample time are chosen according to the telescope motor saturation and hardware, respectively. The prediction and control horizons are chosen such that the open-loop MPC algorithm is solved in a one-time step such that its real-time feasibility is guaranteed. Indeed, it is worth noting that, as N_p increases, the computation burden enlarges. Conversely, the more N_c increases, the less is the number of calls of the open loop MPC algorithm. Finally, the closed-loop MPC algorithm is implemented according to Sec. 3.2.2.

4.3 Performance Analysis

In this section, we disclose the effectiveness of the proposed MPC-based in letting the TNG telescope track the scientific target as well as its robustness w.r.t. input external disturbances and measurement white noises. With the aim of implementing the MPC-based control algorithm in problem $\mathcal{D}$, the derived TNG state space representation, described in Sec. 4.1, is exploited as the prediction model. By leveraging the Yalmip toolbox along with the Mosek optimizer, the MPC closed-loop algorithm is developed according to Sec. 3, with a proper choice of the degree of freedom Q, R, and F reported in Table 2(a).

Conversely, the Kalman filter gain L_∞ is computed according to Eq. (12) with matrices L_e and L_a reported in Table 2(a). The physical constraints involved in the parameter set-up of the trajectory generator are set as in Ref. 22, and they are reported in Table 2(b).

Based on the TNG model identified in Sec. 4.1, by characterizing the von Kármán disturbance model along with the measurement white noise, as in Table 2(c), the virtual testing is performed by exploiting an advanced own-made MATLAB and Simulink simulation platform. This latter exploits a trapezoidal stiffness algorithm solver (ode23t) as an integration method with a sample time of $\Delta t = 0.002[s]$.

The virtual testing procedure involves the following star tracking scenarios: (i) the tracking of the scientific star TYC 1731-916-1; (ii) the tracking of a pseudo star, which forces the TNG to operate near the singularity condition $\vartheta \simeq 89$ deg. Finally, a comparison analysis, w.r.t. a Linear-Quadratic-Gaussian-Proportional-Integrator (LQG-PI)[17] and a PID[12]-based tracking controllers, and a robustness analysis, w.r.t. the model mismatch between the prediction model in Eq. (16b) and plant Eq. (2), highlights the advantages and benefits of the proposed MPC-based control architecture.

Table 2 Simulation set-up.

(a) MPC weighting matrices and Kalman filter observer gain

$$Q = \begin{bmatrix} 2000 & 0 & 0 & 0 \\ 0 & 1500 & 0 & 0 \\ 0 & 0 & 150 & 0 \\ 0 & 0 & 0 & 0.1 \end{bmatrix} \qquad F = \begin{bmatrix} 100 & 0 & 0 & 0 \\ 0 & 50 & 0 & 0 \\ 0 & 0 & 5 & 0 \\ 0 & 0 & 0 & 1 \end{bmatrix}$$

$$L_e = \begin{bmatrix} -2.710 \times 10^{-14} \\ 7.6969 \times 10^{-13} \\ -6.775 \times 10^{-13} \\ -1.284 \times 10^{-12} \\ 4.7708 \times 10^{-11} \\ -1.217 \times 10^{-10} \end{bmatrix} \qquad L_a = \begin{bmatrix} -2.846 \times 10^{-15} \\ -1.388 \times 10^{-16} \\ -1.254 \times 10^{-15} \\ 4.3253 \times 10^{-15} \\ -1.860 \times 10^{-15} \\ -3.040 \times 10^{-5} \end{bmatrix}$$

$$R = \begin{bmatrix} 10^{-4} & 0 \\ 0 & 10^{-6} \end{bmatrix}$$

(b) MPC-based tracking control architecture features

MPC:	$\Delta t = 0.002$[s]	$T_p = 1$[s]	$T_c = 0.002$[s]	$u_{\min} = -500$[Nm]	$u_{\max} = 500$[Nm]
Trajectory generator:	$\Delta t = 0.002$[s]		$v_{\max} = 1.5$[deg /s]	$a_{\max} = 0.1$[deg /s^2]	

(c) von Kármán model parameters and white noise measurement parameters

$f(j) = j\Delta f, j \in (0, D)$	$D = 10{,}000$	$\Delta f = 0.01$[1/s]	$\bar{\tau} = 1$[kN]	$\alpha = 0.35$	$\omega = \mathcal{W}(0, 1.16)$[deg]
$\phi_j = \mathcal{N}(0, 0.5)$	$\mathcal{I} = 0.15$	$\Gamma = 3.2$	$\bar{v} = 3.2$[m/s^2]		$\Lambda = 10$[m^2]

Remark 5: *Note that the resolution of the position encoders equipped on the TNG is* 139,06 arcsec. *However, it is important to remark on two crucial aspects: (i) the real data related to TNG dynamics, used to identify the TNG dynamical model, are obtained via the tachometer measurements with a resolution that is higher than the encoder. Indeed, the conversion factor between the encoder and the related tachometer is 1 encoder count is* $1.1e^{-4}$ [arcsec] *for the related tachometer; (ii) the own-realized simulation platform does not take into account the emulation of the encoder as all the measured physical quantities are derived from the tachometer. This latter point is an essential aspect for better understanding why the results in* Table 3 *are of one order of magnitude less than that ensured by the encoders themselves.*

4.3.1 *Tracking of TYC 1731-916-1*

Considering the TNG observatory, located at latitude 28° 45′ 14″ N and longitude 17° 53′ 17″ W, the scientific star target trajectories of TYC 1731-916-1 are obtained via the astronomical computation with right ascension (RA) of 00:29:50 [hh:mm:ss], declination (DEC) of 23:45:09 (dd:mm:ss) in the observation date 22:03:2024 (dd:mm:yy) at time 13:40:12 (hh:mm:ss). Note that the real scientific star altitude trajectory is within the operative range of the identified TNG model, i.e., $\theta^{\star}(t) \in (80 \text{ and } 90 \text{ deg})$. Moreover, the trajectory generator in Sec. 3.1 computes the admissible telescope trajectories $\bar{y}_p(t) = [\bar{\vartheta}(t), \bar{\varphi}(t)]$ to reach the star in <10 s from the rest position, i.e., initial state condition, $\vartheta(0) = 90$ deg and $\varphi(0) = \kappa\, 360$ [deg] $\forall\, \kappa \in \mathbb{N}$.

The results are depicted in Fig. 4 and disclose the high-tracking performance ensured by the proposed optimal control architecture despite the presence of external disturbance $\delta(t)$ and noise measurements ω. More specifically, Figs. 4(a) and 4(b) show the position trends of the scientific target $y^{\star}(t) = [\vartheta^{\star}(t), \varphi^{\star}(t)]$, the pre-processed trajectories $\overline{y}_p(t) = [\overline{\vartheta}(t), \overline{\varphi}(t)]$, and the telescope positions $[\vartheta(t), \varphi(t)]$, hence confirming the achievement of the control goal Eq. (7a) with small bounded errors [see Fig. 4(g)]. This high-tracking performance is also disclosed in Figs. 4(d) and 4(e). Herein, it highlighted the capability of the proposed solution in ensuring the tracking of the speed measurements $y(t) = [\vartheta(t), \varphi(t)]$ toward the target star velocities, i.e., $\dot{y}^{\star}(t) = [\dot{\vartheta}^{\star}(t), \dot{\varphi}^{\star}(t)]$, and the pre-processed trajectories, i.e., $\overline{y}_s(t) = [\dot{\overline{\vartheta}}(t), \dot{\overline{\varphi}}(t)]$, hence confirming the achievement of the control goal Eq. (7b) with small bounded errors [see Fig. 4(h)]. Moreover, for the sake of completeness, Fig. 4(c) reports the time history of the computed optimal torques $u(t) = [\tau_e(t), \tau_a(t)]$, whereas Fig. 4(f) shows the effectiveness of the Kalman filter in ensuring the convergence of the estimation errors toward zero.

4.3.2 *Psuedo star in singularity condition*

The effectiveness of the MPC-based control architecture is here disclosed by considering the more challenging tracking scenario for a ground-based telescope, namely, the one close to the singularity condition $\vartheta(t) \simeq 90$ deg.

Hence, considering the TNG observatory, the pseudo-scientific star target trajectories are emulated via the astronomical computation with right ascension (RA) of 21:25:00 (hh:mm:ss), declination (DEC) of 27:60:00 (dd:mm:ss) in the observation date 9:10:2023 (dd:mm:yy) at time 20:53:52.72 (hh:mm:ss). In doing so, the altitude of the pseudo star is ∼89 deg, whereas the telescope is in rest position, i.e., $\vartheta(0) = 90$ deg and $\varphi(0) = \kappa\, 360$ deg $\forall\, \kappa \in \mathbb{N}$.

According to the initial setting for the TNG telescope and the scientific target position $\overline{y}_p(t) = [\overline{\vartheta}(t), \overline{\varphi}(t)]$, the trajectory generator, in Sec. 3.1, computes the admissible telescope trajectories to reach the star in less than 50 s. The results are depicted in Fig. 5 and disclose the high-tracking performance ensured by the proposed optimal control architecture despite the presence of external disturbance $\delta(t)$ and noise measurements ω. More specifically, Figs. 5(a) and 5(b) show the position trends of the pseudo star $y^{\star}(t) = [\vartheta^{\star}(t), \varphi^{\star}(t)]$, the pre-processed trajectories $\overline{y}_p(t) = [\overline{\vartheta}(t), \overline{\varphi}(t)]$, and the telescope positions $[\vartheta(t), \varphi(t)]$, hence confirming the achievement of the control goal Eq. (7) with small bounded errors [see Fig. 5(g)]. Moreover, Figs. 5(d) and 5(e), reporting the velocities trends of the pseudo star $\dot{y}^{\star}(t) = [\dot{\vartheta}^{\star}(t), \dot{\varphi}^{\star}(t)]$, the pre-processed

Table 3 Comparison results: TI, RMSE, and improvement (%) w.r.t. LQG-PI[17] and PID.[12]

Axis		$\vartheta(t)$ (arcsec)				$\varphi(t)$ (arcsec)			
Configuration $\vartheta^\star(0)$		78 deg	82 deg	87 deg	89 deg	78 deg	82 deg	87 deg	89 deg
MPC	TI	6.24×10^{-5}	6.24×10^{-5}	5.99×10^{-5}	5.99×10^{-5}	0.125	0.125	0.1164	0.1164
	RMSE	1.02×10^{-4}	1.13×10^{-4}	2.92×10^{-4}	2.92×10^{-4}	2.26×10^{-4}	2.47×10^{-4}	2.11×10^{-4}	2.11×10^{-4}
LQG-PI	TI	100.88	94.655	91.257	98.632	12.245	11.762	11.259	9.422
	Improvement (%)	−99.99	−99.99	−98.63	−98.63	−98.97	−98.93	−98.97	−82.65
	RMSE	0.0084	0.0082	0.0084	0.0191	0.0084	0.0082	0.0084	0.0191
	Improvement (%)	−87.85	−86.21	−96.52	−98.90	−97.30	−96.98	−97.49	−98.90
PID	TI	75.438	71.121	66.962	72.657	47.545	46.874	43.676	34.021
	Improvement (%)	−99.99	−99.99	−99.99	−99.99	−99.73	−99.73	−99.73	−99.66
	RMSE	0.0266	0.0278	0.0278	0.0313	0.0266	0.0278	0.0278	0.0313
	Improvement (%)	−96.16	−96.33	−98.95	−99.07	−99.15	−99.11	−99.24	−99.33

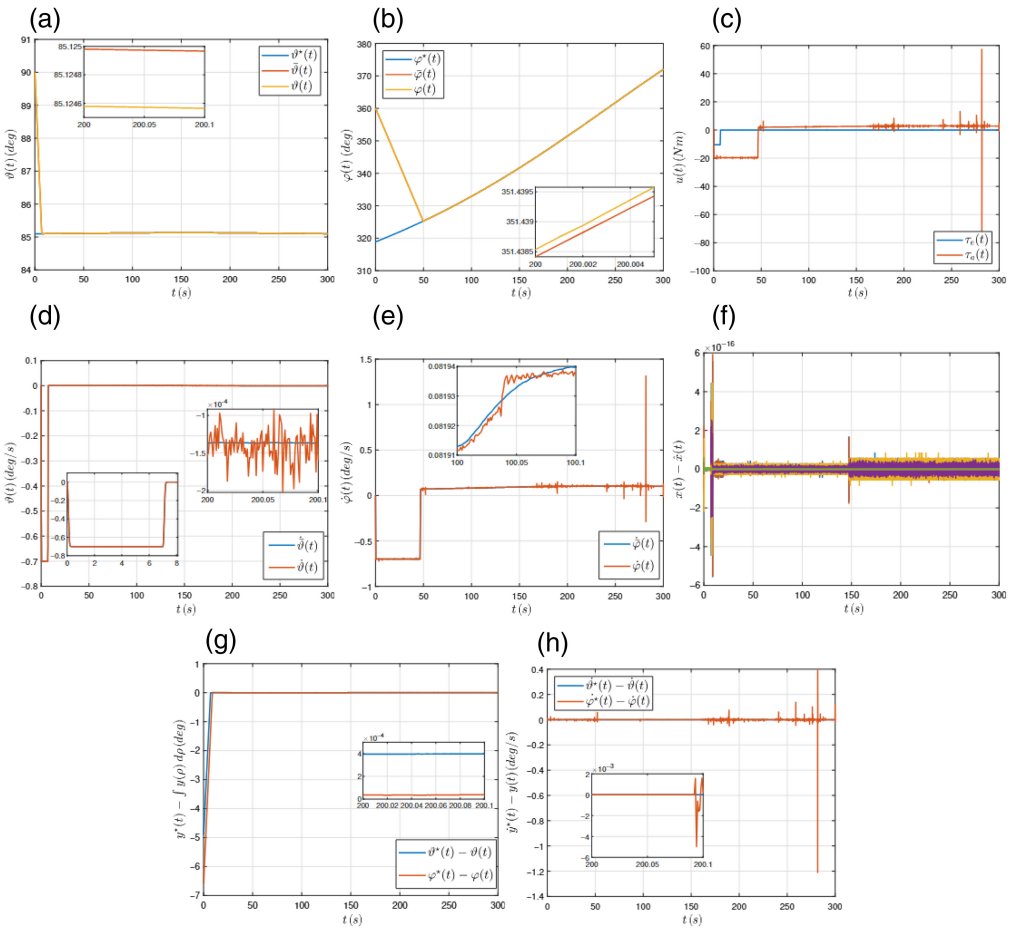

Fig. 4 Performance analysis for the TNG case study. Tracking of TYC 1731-916-1. Time history of (a) altitude position of the star $\vartheta^{\star}(t)$, trajectory generator $\overline{\vartheta}(t)$, and telescope $\vartheta(t)$; (b) the azimuth position of the star $\varphi^{\star}(t)$, trajectory generator $\overline{\varphi}(t)$, and telescope $\vartheta(t)$; (c) optimal control torques $u(t)$; (d) altitude speed of the star $\dot{\vartheta}^{\star}(t)$, trajectory generator $\dot{\overline{\vartheta}}(t)$, and telescope $\dot{\vartheta}(t)$; (e) azimuth speed trajectory $\dot{\overline{\varphi}}(t)$ and telescope speed $\dot{\varphi}(t)$; (f) estimation state errors $x(t) - \hat{x}(t)$ provided by the Kalman filter; (g) tracking position errors $y^{\star}(t) - y_p(t)$; (h) tracking speed errors $\dot{y}^{\star}(t) - y(t)$.

speed trajectories $\overline{y}_s(t) = [\dot{\overline{\vartheta}}(t), \dot{\overline{\varphi}}(t)]$, and the telescope speeds $y(t) = [\dot{\vartheta}(t), \dot{\varphi}(t)]$, show the capability of the MPC-based tracking control in ensuring the speed tracking of the target pseudo star, hence confirming the achievement of the control goal Eq. (7b) with small bounded error [see Fig. 5(h)]. Moreover, for the sake of completeness, Fig. 4(c) reports the time history of the computed optimal torques $u(t) = [\tau_e(t), \tau_a(t)]$, whereas Fig. 4(f) shows the effectiveness of the Kalman filter in ensuring the convergence of the estimation errors toward zero.

4.4 Comparison Analysis

To better highlight the advantages and the benefits of the proposed MPC-based control architecture in solving the tracking telescope control problem, in this section, we compare its closed-loop performance with both the one achievable via the LQG-PI-based double-layer control architecture recently proposed in Ref. 17 and the one obtainable via PID-based control approach in Ref. 12. For more details about the control design, the tuning rules, and the values of the control gains for both the controllers in comparison, see Ref. 17.

The comparison analysis is performed by considering four different pseudo-star trajectories, which are selected such that $\vartheta^{\star}(0)$ is within the operative range of the TNG-identified model, i.e., $\vartheta^{\star}(0) = (78, 82, 87, 89 \text{ deg})$, respectively.

To disclose the improved performance achievable via the proposed approach, the following KPIs are exploited: (i) the tracking index (TI), which evaluates the effectiveness of a controller in

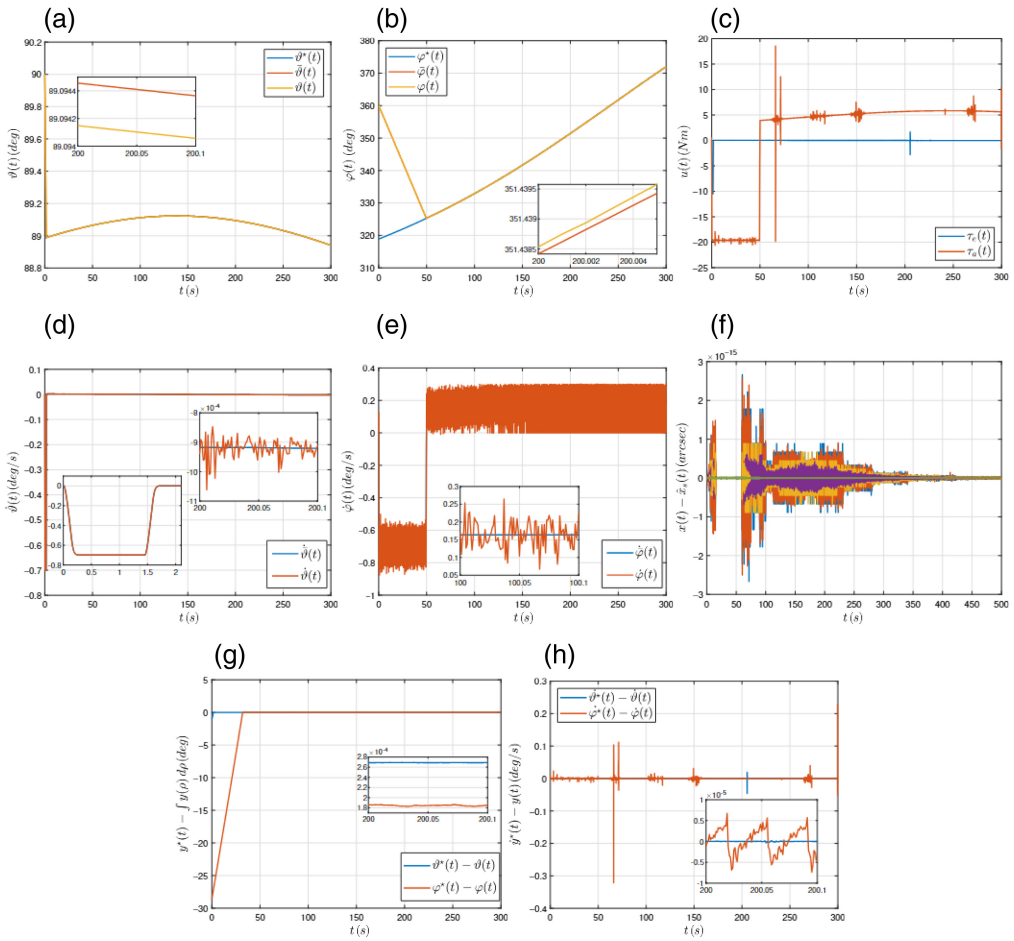

Fig. 5 Performance analysis for the TNG case study. Tracking of the pseudo star in singularity condition. Time history of (a) altitude position of the star $\vartheta^{\star}(t)$, trajectory generator $\overline{\vartheta}(t)$, and telescope $\vartheta(t)$; (b) the azimuth position of the star $\varphi^{\star}(t)$, trajectory generator $\overline{\varphi}(t)$, and telescope $\vartheta(t)$; (c) optimal control torques $u(t)$; (d) altitude speed of the star $\dot{\vartheta}^{\star}(t)$, trajectory generator $\dot{\overline{\vartheta}}(t)$, and telescope $\dot{\vartheta}(t)$; (e) azimuth speed trajectory $\dot{\overline{\varphi}}(t)$ and telescope speed $\dot{\varphi}(t)$; (f) estimation state errors $x(t) - \hat{x}(t)$ provided by Kalman filter; (g) tracking position errors $y^{\star}(t) - y_p(t)$; (h) tracking speed errors $\dot{y}^{\star}(t) - y(t)$.

tracking the reference behavior imposed by a trajectory generator;[32] (ii) the RMSE, which assesses the performance of a controller in tracking the pseudo star at the steady state, that is, after the engagement of this latter.[33]

More specifically, the TI, which weights the speed and position tracking error, is formalized as

$$\mathrm{TI}|_{\vartheta} = \frac{1}{T_s}\int_0^{T_s} |\varpi_p \cdot (\overline{\vartheta}(\rho) - \vartheta(\rho)) + \varpi_s \cdot (\dot{\overline{\vartheta}}(\rho) - \dot{\vartheta}(\rho))| \mathrm{d}\rho, \tag{22}$$

$$\mathrm{TI}|_{\varphi} = \frac{1}{T_s}\int_0^{T_s} |\varpi_p \cdot (\overline{\varphi}(\rho) - \varphi(\rho)) + \varpi_s \cdot (\dot{\overline{\varphi}}(\rho) - \dot{\varphi}(\rho))| \mathrm{d}\rho, \tag{23}$$

where ϖ_p and ϖ_s are positive weights that represent the sensitivity to the position and the velocity error and are set as $\varpi_p = 1$ and $\varpi_s = 10$.

Conversely, for the computation of the RMSE, we take into account the time windows starting from $t_0 = 100[\mathrm{s}]$, namely, the time required by the pre-processed trajectories in engaging the target star, until the end of the simulation scenario, i.e., the simulation time $T_s = 300[s]$. Hence, the RMSE, for both position trajectories, is equated as

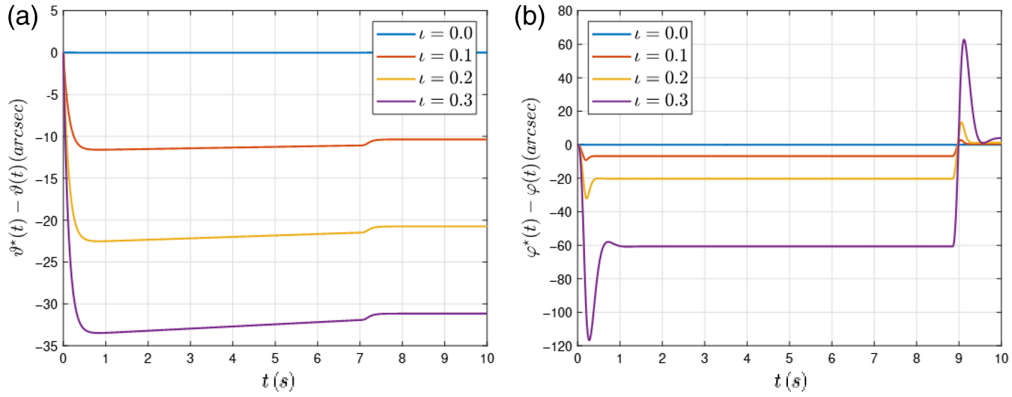

Fig. 6 Robustness analysis of the proposed MPC-based control architecture w.r.t. 10%, 20%, and 30% model mismatch, that is, $\iota = 0.1, 0.2, 0.3$, respectively. Time history of (a) altitude position error $\overline{\vartheta}(t) - \vartheta(t)$ and (b) azimuth position error $\overline{\varphi}(t) - \varphi(t)$.

$$\text{RMSE}|_{\vartheta} = \frac{1}{T_s - t_0} \int_{t_0}^{T_s} \|\vartheta^\star(\rho) - \vartheta(\rho)\|_2 \mathrm{d}\rho, \tag{24}$$

$$\text{RMSE}|_{\varphi} = \frac{1}{T_s - t_0} \int_{t_0}^{T_s} \|\varphi^\star(\rho) - \varphi(\rho)\|_2 \mathrm{d}\rho. \tag{25}$$

Comparison results, reported in Table 3, demonstrate the high performance achieved and the improvement of the MPC-based tracking control w.r.t. both the LQG-PI and the PID-based architectures in terms of TI and RMSE, despite the presence of external disturbance $\delta(t)$. Furthermore, as shown in the RMSE-improved performance, the proposed strategy is able to properly reject the noise measurement and hence ensure a precise tracking of the appraised scientific star target.

4.5 Robustness Analysis

Herein, with the aim of demonstrating the benefits and the drawbacks of the proposed MPC-based control architecture, we present a robustness analysis w.r.t. the model mismatch between the prediction model in Eq. (16b), exploited for solving the open-loop optimal problem in $\mathcal{D}$, and the TNG plant in Eq. (2).

In doing so, as in Ref. 34, the model mismatch is taken into account by considering the following inertial matrix $A = A + \iota A$ being A the nominal inertial matrix reported in Table 1 while $\iota \in (0, 1)$ representing the uncertainties. The tracking of TYC 1731-916-1 is selected as a simulation scenario, and to better highlight the robustness of the model mismatch, no wind disturbance is considered, i.e., $\delta(t) = 0$. Moreover, the simulation time is set to $T_s = 10$[s]. We consider model uncertainties of 10%, 20%, and 30%, i.e., $\iota = 0.1, 0.2, 0.3$, respectively. The KPIs, described in Sec. 4.4, are exploited to assess the benefits/limitations of the proposed MPC-based control architecture.

Simulation results are reported in Fig. 6, where the error position trend for the altitude and azimuth axes is disclosed in Figs. 6(a) and 6(b), respectively. From them, it is possible to observe that, although the proposed architecture performances are slightly downgraded (as the model mismatch between the prediction model increases), the star tracking is still ensured with small bounded errors. This is also confirmed by the performed TI and RMSE indexes reported in Table 4.

5 Conclusions

In this paper, the optimal tracking control problem for a ground-based telescope in the presence of noise measurements and external disturbances has been addressed. A novel MPC-based control architecture, comprehensive of a trajectory generator for ensuring the physical constraints of the telescope, and an infinite horizon Kalman filter to properly mitigate the measurement noise, has been proposed. The solution has been tailored for the TNG telescope located at "Roque de los Muchacho," La Palma (Spain). To this end, by leveraging real telescope data, the TNG dynamical

Table 4 Robustness analysis results: TI, RMSE w.r.t. model mismatch of 10%, 20%, and 30%, that is, $\iota = 0.1, 0.2, 0.3$.

	TI		RMSE	
ι	$\vartheta(t)$	$\varphi(t)$	$\vartheta(t)$	$\varphi(t)$
0.0	2.23×10^{-4}	1.29×10^{-4}	2.42×10^{-4}	1.04×10^{-4}
0.1	0.0102	0.0058	0.0058	0.0018
0.2	0.0204	0.0176	0.0195	0.0054
0.3	0.0306	0.05318	0.1429	0.0165

behavior has been identified via the non-iterative subspace approach. Based on that, the proposed MPC-based controller plus a Kalman filter have been developed via Yalmip-tool and Mosek optimizer in MATLAB environment. The effectiveness of the proposed solution in ensuring the optimal star tracking of the TNG telescope has been disclosed via virtual simulation, carried out via an advanced own-made MATLAB and Simulink platform, for different star tracking scenarios, also involving the real scientific target TYC 1731-916-1. The results prove the capability of the architecture in achieving the control goals with high tracking performance despite the presence of external disturbances and measurement noise with significant improvements w.r.t. state-of-the-art control strategies.

Finally, future works include (i) the improvement of the identification procedure to overcome the limitation stated in remark 4 while also enlarging the TNG operative range, i.e., 15 and 89 deg; (ii) extension of the own-realized MATLAB-based simulation platform by including dedicated modules emulating the TNG sensors behavior and limitations. In doing so, the test and the validation of the proposed MPC-based control architecture on the real TNG telescope can be performed as final future work.

Code and Data Availability

The data supporting the findings of this study as well as the developed control algorithm are openly available at MPC-tracking-4-Ground-Based-Telescope at the link https://github.com/GiacomoBasile/MPC-tracking-4-Ground-Based-Telescope.git.

References

1. T. Tang et al., "A review on control methodologies of disturbance rejections in optical telescope," *Opto-Electron. Adv.* **2**(10), 190011 (2019).
2. W. Gawronski, "Control and pointing challenges of antennas and telescopes," in *Proc. Amer. Control Conf.*, IEEE, pp. 3758–3769 (2005).
3. P. Schipani et al., "The tracking control system of the VLT survey telescope," *Rev. Sci. Instrum.* **83**(9), 094501 (2012).
4. W. Gawronski, "Control and pointing challenges of large antennas and telescopes," *IEEE Trans. Control Syst. Technol.* **15**(2), 276–289 (2007).
5. M. Ravensbergen, "Main axes servo systems of the VLT," *Proc. SPIE* **2199**, 997–1005 (1994).
6. T. Erm and P. Gutierrez, "Integration and tuning of the VLT drive systems," *Proc. SPIE* **4004**, 490–499 (2000).
7. M. Suárez et al., "The GTC main axes servos and control system," *Proc. SPIE* **7019**, 70190J (2008).
8. D. Mancini, E. Cascone, and P. Schipani, "Italian national Galileo telescope (TNG) system description and tracking performance in the workshop," *Proc. SPIE* **3086**, 85–95 (1997).
9. D. Mancini, E. Cascone, and P. Schipani, "Telescope control system stability study using a variable structure controller," *Proc. SPIE* **3351**, 331–341 (1998).
10. T. Bretz et al., "The drive system of the major atmospheric gamma-ray imaging Cherenkov telescope," *Astropart. Phys.* **31**(2), 92–101 (2009).
11. W. Gawronski, "Servo-performance parameters of the NASA deep space network antennas," *IEEE Antennas Propag. Mag.* **49**(6), 40–46 (2007).

12. D. MacMynowski, C. Blaurock, and G. Angeli, "Initial control results for the thirty meter telescope," in *AIAA Guid. Navig. and Control Conf. and Exhibit.*, p. 6075 (2005).
13. B. Sedghi et al., "Main axes control of E-ELT," *Proc. SPIE* **7733**, 77331G (2010).
14. E. White et al., "Green bank telescope: overview and analysis of metrology systems and pointing performance," *Astron. Astrophys.* **659**, A113 (2022).
15. O. Keskin et al., "Modelling and simulation studies on adaptive controller for alt-azimuth telescopes despite unknown wind disturbance and mass," *Adv. Mech. Eng.* **12**(9), 1687814020954767 (2020).
16. F. Allgöwer and A. Zheng, *Nonlinear Model Predictive Control*, Vol. **26**, Birkhäuser (2012).
17. G. Basile et al., "Model-based optimal tracking control architecture for ground-based telescopes," *Proc. SPIE* **13094**, 130943L (2024).
18. W. Gawronski, *Modeling and Control of Antennas and Telescopes*, Springer Science & Business Media (2008).
19. P. Schipani and D. Mancini, "Modeling the VST telescope and the effect of the wind disturbance on its performance," *IFAC Proc.* **35**(1), 179–185 (2002).
20. M. Olberg et al., "Simple, robust digital controller for the Onsala 20-m radio telescope," *Proc. SPIE* **2479**, 257–265 (1995).
21. S. Sandrock et al., "Design and implementation of a general main axis controller for the ESO telescopes," *Proc. SPIE* **8451**, 226–237 (2012).
22. S. Savarese et al., "Trajectory generation methods for radio and optical telescopes," *Proc. SPIE* **11445**, 1144553 (2020).
23. G. L. Serra, *Kalman Filters: Theory for Advanced Applications*, BoD–Books on Demand (2018).
24. Y. Zheng et al., "Distributed model predictive control for heterogeneous vehicle platoons under unidirectional topologies," *IEEE Trans. Control Syst. Technol.* **25**(3), 899–910 (2016).
25. H. Chen and F. Allgöwer, "A quasi-infinite horizon nonlinear model predictive control scheme with guaranteed stability," *Automatica* **34**(10), 1205–1217 (1998).
26. J. Köhler, M. A. Müller, and F. Allgöwer, "A nonlinear tracking model predictive control scheme for dynamic target signals," *Automatica* **118**, 109030 (2020).
27. S. Morales et al., "LQR trajectory tracking control of an omnidirectional wheeled mobile robot," in *IEEE 2nd Colombian Conf. on Robot. and Automat. (CCRA)*, pp. 1–5, IEEE (2018).
28. P. Schipani et al., "Towards new servo control algorithms at the TNG telescope," *Proc. SPIE* **11445**, 1144552 (2020).
29. A. Ghedina et al., "Three years of dust monitoring at the Galileo telescope," *Proc. SPIE* **5489**, 227–234 (2004).
30. A. K. Tangirala, *Principles of System Identification: Theory and Practice*, CRC Press (2018).
31. M. Gonzalez et al., "Telescopio Nazionale Galileo control system upgrade," *Proc. SPIE* **13094**, 1309441 (2024).
32. A. Coppola et al., "Eco-driving control architecture for platoons of uncertain heterogeneous nonlinear connected autonomous electric vehicles," *IEEE Trans. Intell. Transp. Syst.* **23**(12), 24220–24234 (2022).
33. T. O. Hodson, "Root-mean-square error (RMSE) or mean absolute error (MAE): when to use them or not," *Geosci. Model Dev. Discuss.* **15**, 5481–5487 (2022).
34. A. S. Badwe et al., "Detection of model-plant mismatch in MPC applications," *J. Process Control* **19**(8), 1305–1313 (2009).

Giacomo Basile received his MS degree in automation engineering from the University of Naples Federico II in 2020. Now he is a PhD student in Information Technology and Electrical Engineering, Cycle: XXXVII. His research interests include artificial intelligence controller in autonomous drive field and adaptive optics system for very large telescope (VLT) and extremely large telescope (ELT) in collaboration with observatory of naples capodimonte.

Manuel Gonzalez is the technical coordinator at Telescopio Nazionale Galileo, a 3.6-meter Italian telescope located in the Canary Islands, Spain. He earned a degree in electronics engineering from La Laguna University (Tenerife, Spain) in 1999, and has dedicated his entire professional career to astronomy. His work focuses mainly on real-time systems, control systems, instrumentation, and electronics design.

Alberto Petrillo is an assistant professor of Systems and Control Engineering and chief technical officer of the Distributed Automation System Lab at the University of Napoli Federico II. He received his PhD in control systems engineering from University of Napoli Federico II in 2019. His research activity concerns both theoretical and application topics in the automatic control field and combines the methodological aspects with experimental validation.

Stefania Santini is professor of Systems and Control Engineering at the University of Naples Federico II. She leads the Distributed Automation Systems Lab. Her research interests include nonlinear control, time-delayed systems, and networked and multi-agent systems, applied to automotive, transportation, and energy. She is senior editor of IEEE Transactions on Intelligent Transportation Systems, associate editor of IEEE Transactions on Control Systems Technology, and vice-chair of IEEE ITS Italian Chapter. She is principal investigator of national/international research projects.

Salvatore Savarese received his PhD in Information Technology and Electrical Engineering from the University of Naples "Federico II," in 2018. In 2020, he won a postdoctoral position at Instituto Nazionale di Astrofisica (INAF) of Naples. Since 2022, he is a staff Technologist at the same institute. His main research interests involve the instrument control systems for ground-based telescopes, and RTC systems for adaptive optics instruments.

Pietro Schipani is a director of research in Technology at INAF (Italy). His research focuses on design and realization of astronomical telescopes and instrumentation. He is director of INAF–Capodimonte Astronomical Observatory.